Investigating the dielectric properties and exciton diffusion in C70 derivatives

Rousseva, Sylvia; Raul, Benedito A L; van Kooij, Felien S; Kuevda, Alexey V; Birudula, Srikanth; Hummelen, Jan C; Pshenichnikov, Maxim S; Chiechi, Ryan C

Published in:
PPCP : Physical Chemistry Chemical Physics

DOI:
10.1039/d2cp00791f

Publication date:
2022

PCCP

PAPER

View Article Online
View Journal | View Issue

Cite this: *Phys. Chem. Chem. Phys.*, 2022, **24**, 13763

Investigating the dielectric properties and exciton diffusion in C_{70} derivatives†

Sylvia Rousseva,[ab] Benedito A. L. Raul,[b] Felien S. van Kooij,[ab] Alexey V. Kuevda,[b] Srikanth Birudula,[ab] Jan C. Hummelen,[ab] Maxim S. Pshenichnikov *[b] and Ryan C. Chiechi *[ac]

In recent years, the dielectric constant (ε_r) of organic semiconductors (OSCs) has been of interest in the organic photovoltaic (OPV) community due to its potential influence on the exciton binding energy. Despite progress in the design of high ε_r OSCs and the accurate measurement of the ε_r, the effects of the synthetic strategies on specific (opto)electronic properties of the OSCs remain uncertain. In this contribution, the effects of ε_r on the optical properties of five new C_{70} derivatives and [70]PCBM are investigated. Together with [70]PCBM, the derivatives have a range of ε_r values that depend on the polarity and length of the side chains. The properties of the singlet excitons are investigated in detail with steady-state and time-resolved spectroscopy and the exciton diffusion length is measured. All six derivatives show similar photophysical properties in the neat films. However, large differences in the crystallinity of the fullerene films influence the exciton dynamics in blend films. This work shows that design principles for OSCs with a higher ε_r can have a very different influence on the performance of traditional BHJ devices and in neat films and it is important to consider the neat film properties when investigating the optoelectronic properties of new materials for OPV.

Received 16th February 2022,
Accepted 19th April 2022

DOI: 10.1039/d2cp00791f

rsc.li/pccp

1 Introduction

Since the first use of [6,6]-Phenyl-C61-butyric acid methyl ester ([60]PCBM) in bulk heterojunction (BHJ) solar cells,[1] the fullerene derivative and its C_{70} analogue ([70]PCBM) have been used extensively in organic photovoltaics (OPVs) and other organic electronic devices. The main benefit of using PCBM compared to the parent fullerene is its enhanced solubility in organic solvents, allowing for films to be processed from solution rather than through vacuum deposition. Furthermore, PCBM shares many of the properties of its parent fullerene, such as high electron mobility together with a low lying lowest unoccupied molecular orbital (LUMO) and unusual 3D structure; allowing it to be a favourable electron acceptor and exhibit n-type semiconductor behaviour. These properties contributed to its establishment as a work horse of the early OPV community. Much of the physics underlying the processes occurring in organic solar cells was established from experiments on the prototypical poly(3-hexylthiophene-2,5-diyl) (P3HT):[60]PCBM bulk heterojunction system, that can achieve an optimised power conversion efficiency (PCE) of 5.4%.[2] Other fullerene derivatives with various aryl groups, side chains and end groups, as well as bis-adducts have been investigated in BHJs, in particular with the aim of controlling the open circuit voltage (V_{oc}) and hence improving PCEs.[3] However, although time resolved spectroscopic studies have been carried out on PCBM films,[4–8] spectroscopic investigations of other C_{60} and C_{70} derivatives are rare in the literature.

As part of our ongoing efforts to design high dielectric constant (ε_r) organic semiconductors (OSCs), with the aim of moving away from BHJ solar cells towards single semiconductor organic photovoltaics (SSC-OPVs), we decided to investigate how the choice of side chains in our fullerene derivatives may influence the photophysical properties specifically. We chose to study C_{70} derivatives as they absorb more strongly in the visible range of the spectrum compared to C_{60} due to the reduced symmetry of the higher fullerene which relaxes the symmetry-forbidden nature of the electronic transitions. Furthermore, C_{70} derivatives have been investigated as the main component in dilute-donor solar cells where they exhibit ambipolar charge-transport behaviour[9,10] and also remain important components of high efficiency ternary blend solar cells.[11]

[a] *Stratingh Institute for Chemistry, University of Groningen, Nijenborgh 4, 9747 AG Groningen, The Netherlands*
[b] *Zernike Institute for Advanced Materials, Nijenborgh 4, 9747 AG Groningen, The Netherlands. E-mail: m.s.pchenitchnikov@rug.nl*
[c] *Department of Chemistry, North Carolina State University, Raleigh, North Carolina 27695-8204, USA. E-mail: ryan.chiechi@ncsu.edu*

† Electronic supplementary information (ESI) available: Synthesis and material characterisation, NMR spectra, MC simulation parameters; UV-Vis absorption spectra, PL decays and AFM images of blend films. See DOI: https://doi.org/10.1039/d2cp00791f

Although the dielectric properties of OSCs are a significant research topic, much remains to be understood about the effect of ε_r on the photophysics and optoelectronic properties of OSCs in the solid state. With regard to OPVs, due to the nature of electrostatic forces, the ε_r of the active layer may directly affect the exciton binding energy, the singlet–triplet gap and both geminate and non-geminate recombination in OPV devices.[12,13] One strategy that has been explored for increasing ε_r is the use of side chains with embedded permanent dipoles that can reorient in the film. This technique changes the ε_r of the material in the so called low-frequency regime ($<10^6$ Hz) with movement of the dipoles occuring on time scales of 1 μs to 1 s. A wide range of OSCs with various side chains have been synthesised and the low-frequency dielectric constant (ε_r^{lf}) measured.[14–16] However, the use of these modified ε_r^{lf} OSCs in BHJ solar cells has not directly correlated to improvements in the PCE.

In contrast, Xu *et al.* investigated a series of donor polymers with and without polar cyano-groups in the side chains, and found that the cyano-groups were detrimental to the PCE of BHJ devices based on blends of the polymer and [70]PCBM.[17] The reason was determined to be a decrease in the hole mobility of the polymers with cyano-groups caused by trap-states formed by the local dipoles in the film. In another study, Hughes and coworkers compared the performance and recombination dynamics of a glycolated C_{60} derivative, TEG-[60]PCBM where TEG refers to triethylene glycol, and [60]PCBM in BHJ solar cells.[18] They found an increase in Shockley–Read–Hall (trap-assisted) recombination and a decreased dissociation efficiency for the solar cells with TEG-[60]PCBM and concluded that small differences in ε_r did not significantly reduce the loss processes in the BHJs.

Meanwhile in neat films, some small molecule materials with ethylene glycol (EG) side chains have shown improved external quantum efficiency (EQE) relative to their lower ε_r analogues with alkyl side chains.[19] Furthermore, several studies have shown that in neat films, the hole (electron) mobility of glycolated donor (acceptor) materials has remained the same relative to the reference material, or even improved.[14,15] Since morphology is a key factor in the PCEs of BHJ solar cells, it remains a question whether high ε_r materials with dipolar side chains have very different processing requirements for optimised performance or whether the permanent dipoles themselves cause fundamental problems in device performance.

It is also worth noting that it is unclear which frequency regime is most important for considering the effects of ε_r on OPV performance.[20] Whilst carrier transport occurs in the micro-second–nanosecond range, for exciton dynamics, the timescales are often on the order of picoseconds ($\sim 10^{-12}$). The rise of high efficiency non-fullerene acceptors (NFAs) with their large planar π -systems has led to renewed discussion on the role of the polarisability or the so called optical/high frequency ε_r^{opt} (10^{12}–10^{14} Hz).[21–23]

To learn more about the effects of changing ε_r, we investigated the photophysical properties of [70]PCBM and five new C_{70} derivatives with different side chain lengths and polarities. After characterisation of the dielectric properties, the materials were studied with steady state and time-resolved spectroscopy and the exciton diffusion length was measured. We focus on the singlet exciton dynamics for this study and find that although the polarity of the side chains influences the dielectric properties, the properties of the singlet exciton are largely uninfluenced.

2 Results and discussion

To investigate the influence of the side chain polarity on the properties of the C_{70} fullerene core, we synthesised five new C_{70} derivatives (Fig. 1 and Scheme S1, ESI†). The materials can be separated into two groups with [70]PCBM and BC10-2 on one side with their non-polar side chains, and PCBM-TEG, BDEG-2, BTEG-2 and BTrEG-2 all containing various lengths of polar EG side chains. PCBM-TEG was synthesised in one step through transesterification of the commercially available [70]PCBM. The other four derivatives, B*n*EG-2 (n = 2–4) and BC10-2 were synthesised in two steps: first the desired malonate was obtained through Steglich esterification of malonic acid, and then reacted with C_{70} *via* the Bingel reaction. It is important to note that unlike the case of C_{60}, the reactive [6,6] double bonds in C_{70} are not geometrically equivalent which may result in a mixture of isomers for the mono-adduct. In the case of the methanofullerene [70]PCBM, the resulting product consists principally of the α-isomer (88%) and the two β-type diastereomers (12%).[24] Although some studies have been carried out on the performance of the separated isomers on OPV devices,[25] [70]PCBM is generally used as an isomeric mixture due to the difficulty of separation. In contrast, the Bingel reaction is very selective and results exclusively in one isomer, which could be confirmed from the ^{1}H NMR data (Fig. S3–S7, ESI†) and is known in the literature.[26,27] For this reason we investigate both polar and non-polar derivatives of both families of fullerene

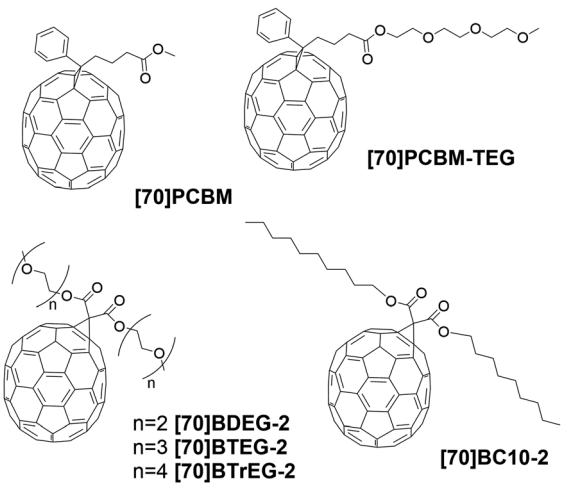

Fig. 1 Chemical structures of the five C_{70} derivatives synthesised for this study together with [70]PCBM. For BDEG-2, BTEG-2, BTrEG-2 and BC10-2, the 'B' refers to the Bingel reaction.

Table 1 Material properties of the fullerene derivatives studied in this work

Material	E_{LUMO} [a] [eV]	ε_r^{opt}	ε_r^{lf}	E_g^{opt} [b] [eV]	λ_{em}^{max} [nm eV^{-1}]	τ_f^{film} [ps]	σ_{PL} [meV]
[70]PCBM	−3.9[c]	3.8–4.9	4.75 ± 0.15[c]	1.71	708/1.75	550	~25
PCBM-TEG	−3.75	3.5–4.6	4.8 ± 0.2	1.71	710/1.75	550	~25
BDEG-2	−3.72	3.5–4.7	6.6 ± 0.6	1.74	699/1.77	550	~25
BTEG-2	−3.75	3.2–4.3	7.0 ± 0.5	1.74	698/1.78	550	~25
BTrEG-2	−3.77	3.3–4.4	7.8 ± 0.3	1.74	700/1.77	550	~25
BC10-2	−3.66	3.1–4.3	3.9 ± 0.2	1.76	689/1.80	550	~25

[a] Estimated from CV measurements in solution with ferrocene as reference. [b] Determined from the onset of absorption in the UV-vis absorption spectra of neat films. [c] From literature.[30] The ε_r^{opt} has been calculated from the complex refractive index using the relation $\varepsilon_r = n^2 - \kappa^2$, the maximum and minimum values from the spectral range (400–1700 nm are given). ε_r^{lf} is given as the average value of the devices measured with impedance spectroscopy, with the standard deviation as the uncertainty.

adducts in this work, rather than comparing a 'non-polar' methano-fullerene to a 'polar' Bingel adduct.

After full characterisation of the synthesised fullerenes, with ^{1}H NMR, ^{13}C NMR, HR-MS, FT-IR and LC-MS (ESI†), the dielectric properties were investigated. Since ε_r is frequency dependent, both the ε_r^{lf} using impedance spectroscopy and the high frequency ε_r^{opt} using ellipsometry were measured. For impedance spectroscopy, parallel plate capacitors were fabricated with the device architecture ITO/PEDOT:PSS/fullerene (100–150 nm)/Al. This sandwich type structure was used so as to emulate conditions in conventional OPV devices. However, in order to obtain clear results, no reactive interlayers, such as LiF, that might dope the fullerene layer were used.[28] Furthermore, the surface morphology was checked for each sample using AFM and devices of different thickness, with low root mean square roughness (σ_{RMS}) values were tested in order to minimise the effects of surface roughness on the measured capacitance.[29]

The capacitance was obtained from the measured impedance by equivalent circuit fitting, and ε_r was calculated using the parallel plate capacitor equation (Section S6.1, ESI†). In accordance with our expectations and previous work, introducing permanent dipoles into the side chain increases the (ε_r^{lf}) of the films (Table 1 and Fig. 2). For the methano-fullerenes, [70]PCBM and PCBM-TEG, the effect of the EG chain was very small. However, for the Bingel series, BC10-2 with alkyl side chains had a much lower ε_r^{lf} than the B*n*EG-2 series with EG side chains. Similarly to our work on the C_{60} Bingel series,[31] increasing the length of the side chains also lead to a gradual increase in the ε_r^{lf}, albeit much smaller in the case of the C_{70} Bingel series.

The ε_r^{opt} of the C_{70} derivatives in neat films was also measured using ellipsometry. In the optical frequency range, the ε_r is related to the optical constants of the material: the refractive index (n) and extinction coefficient (κ). n and κ represent the real and imaginary part of the complex refractive index ($\tilde{n}$) and are related *via* the Kramers–Kronig relations. The optical constants for the different C_{70} derivatives were obtained by fitting the ellipsometry data using a dispersion model constructed using the WVASE software (Section S6.2, ESI†). This involved fitting the extinction coefficient spectrum with multiple Gaussian functions to model the optical transitions in the material, with an approach similar to the work of Aboura *et al.*[32] The optical constants represent the real and imaginary

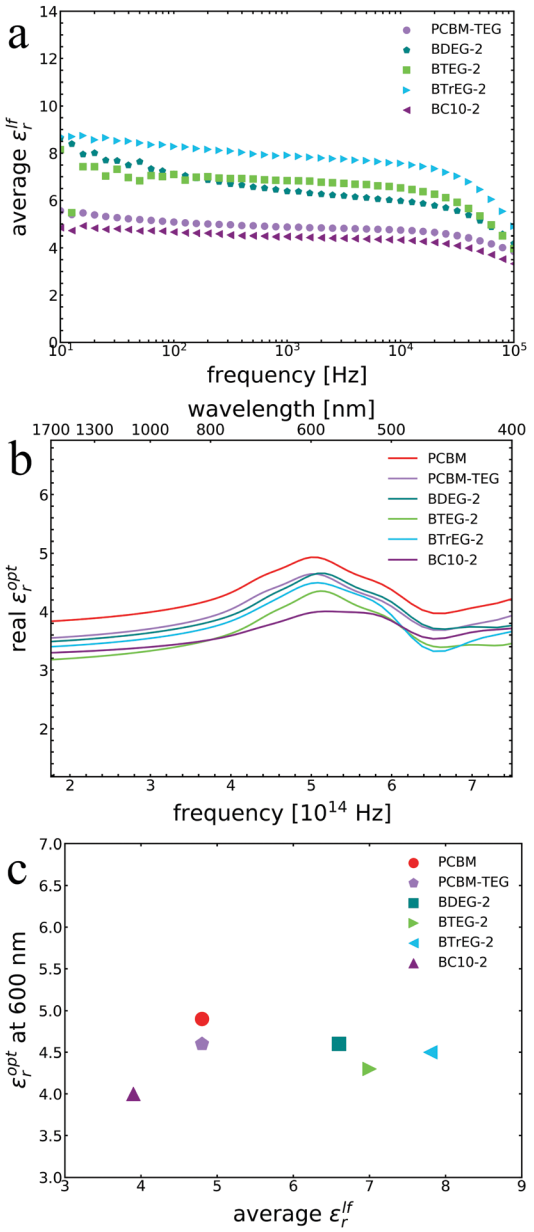

Fig. 2 Dielectric properties of the C_{70} derivatives. (a) The low frequency ε_r obtained by measuring the capacitance with impedance spectroscopy, (b) the optical ε_r calculated from the optical constants of neat films measured by ellipsometry and (c) a correlation plot showing the average ε_r^{lf} and ε_r^{opt} at 600 nm (2.06 eV or 5 × 10^{14} Hz).

part of the complex refractive index, $\tilde{n} = n + i\kappa$ which can be related to ε_r through Maxwell's relations giving $\tilde{\varepsilon}_r = \tilde{n}^2$. The dispersion model was first tested with the data for [70]PCBM and the values obtained for the refractive index were in line with previous literature reports.[21,32] Overall, it was found that increasing the length and number of side chains lead to a lower refractive index across the measured spectral range and hence lower ε_r^{opt}. For the EG series, this meant that increasing length of the side chains, and hence increasing the ε_r^{lf} led to a decrease in the ε_r^{opt}. Since our measurement techniques probe the bulk behaviour of the fullerene films, this relationship shows that in line with theoretical work,[20] when varying the volume fraction ratio of the polarisable conjugated system to the permanent dipole containing aliphatic side chains, in practise there is a trade off between ε_r^{lf} and ε_r^{opt} in the bulk film. Although the change in ε_r^{opt} is much smaller in comparison to the effect of the increasing length of EG chain on the ε_r^{lf}, the balance may be an important consideration in the design of OSCs. The results are concluded in Fig. 2 and Table 1.

Despite the large variations in ε_r, the steady state absorption and photoluminescence spectra of the six derivatives were very similar (Fig. 3). The absorption onset in solution of the methanofullerenes was red shifted compared to the Bingel adducts, and the absorbance peak at ~375 nm is more pronounced, perhaps due to the higher symmetry of the latter or due to the contribution of molecular orbitals delocalised onto the phenyl-ring in the former. Moving from solution to solid state, the peaks are broadened and absorption is enhanced in the visible range (500–700 nm) due to intermolecular interactions.

The photoluminescence (PL) was then measured in solution, in a poly(methyl-methacrylate) (PMMA) matrix and in neat films using an excitation wavelength (λ_{exc}) of 550 nm. (Fig. 4 and Fig. S10, ESI†) The PL emission was weak, with a maximum at ~700 nm (1.77 eV), which has been shown to correspond to emission from the S_1–S_0 transition in fullerene derivatives.[33] The solution and PMMA dispersions exhibited very similar PL spectra, showing a lack of influence from conformational changes to the PL of the fullerenes in solution.[34] There is a small blue shift (~0.05 eV or 10 nm) in the emission of the Bingel series relative to the methano-fullerenes, both in solution and in the films, with the largest blue shift in the case of BC10-2 (Fig. 3). This shift indicates a reduced delocalisation, perhaps due to differences in the electron-withdrawing effect of the adduct group, which has been shown to influence the distribution of the frontier molecular orbitals in theoretical calculations.[5] The larger blue shift in the neat films may additionally suggest weaker intermolecular interactions between the fullerenes in the solid state. Since the strengths of dipole–dipole interactions and London dispersion forces depend on the ε_r of the medium and the polarisability of the molecules, this shift may also be a consequence of the changing dielectric properties.

Moving to time-resolved spectroscopy, the excited state dynamics of the fullerene derivatives were measured in solution, dispersed in PMMA and in neat films (Fig. 4 and Fig. S11, ESI†). The fluorescence lifetimes (τ_f) were obtained by integrating the PL map across the measured spectral range (1.4–2 eV) and fitting the resulting PL transient with a mono-exponential decay

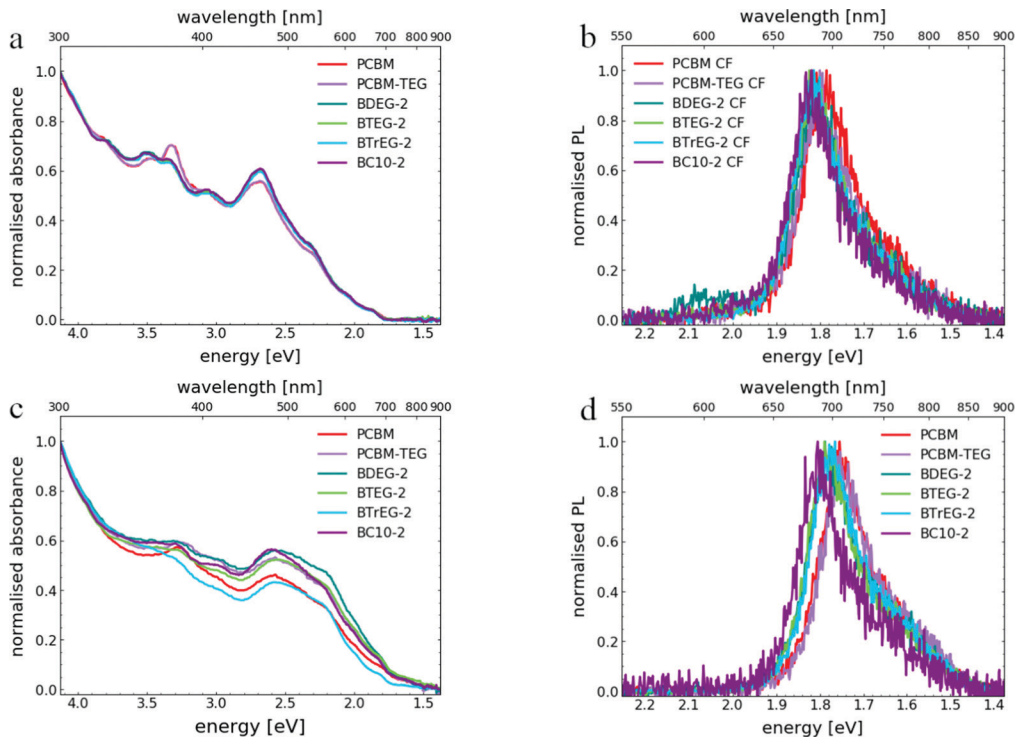

Fig. 3 UV-Vis absorption and fluorescence spectra of the C_{70} derivatives in solution (a and b) and in neat films (c and d). The solution spectra were measured in 10 μm chloroform (CF) solutions.

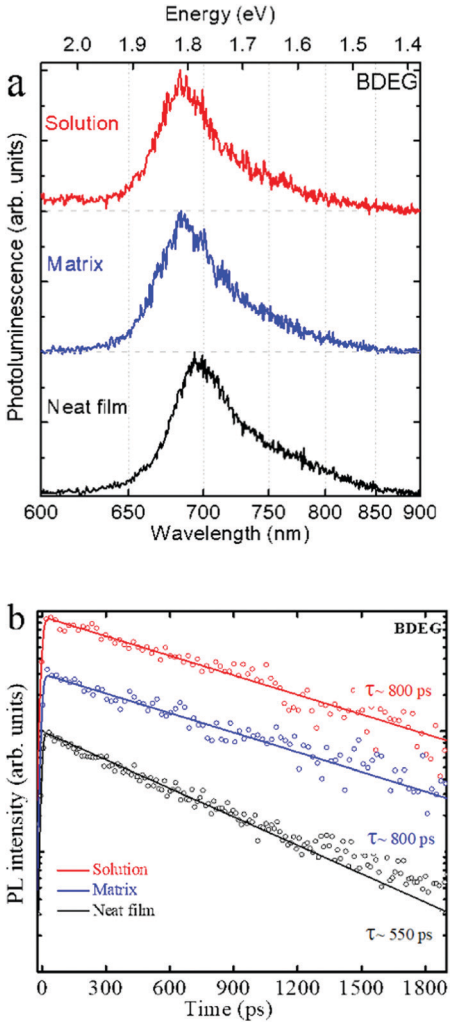

Fig. 4 PL spectra (a) and PL decays (b) of BDEG-2 in CF solution, PMMA matrix and neat film. The spectra for the remaining derivatives are almost identical and are depicted in Fig. S10 and S11 (ESI†).

function convoluted with a Gaussian apparatus function. The PL of all six derivatives exhibited mono-exponential decay, with values of $\tau_f \sim 800 \pm 50$ ps in solution/PMMA matrix and $\tau_f \sim 550 \pm 50$ ps for the neat films (Fig. S11, ESI†). No correlation to the dielectric properties was observed.

Furthermore, the energetic disorder extracted from the PL mean energy shift (Fig. 5) over time was very low (~25 meV, on the order of k_BT) and no significant difference occured when the polarity of the side chain was changed. It has been postulated that side chains with permanent dipoles lead to lower PCE in OPV devices due to increased energetic disorder,[17] however, in the case of the C_{70} derivatives studied in this work, no correlation is seen between the EG chains and the energetic disorder, at least at room temperature.

After fully characterising the photophysical and dielectric properties, we turned our attention to the exciton diffusion length (L_D), another important parameter for organic photovoltaics. The technique of choice for determining the exciton diffusion length was the PL volume-quenching method, in conjunction with Monte-Carlo simulations. For this technique, the material of interest is mixed with a small amount of another material that behaves as an exciton quencher. The PL decay is then measured, and an acceleration in the PL decay is observed due to diffusion-limited dynamic quenching of the excitons. This method alleviates the difficulties involved in controlling the thickness of the films and intercalation at the interface, which is necessary in the case of surface/bilayer quenching techniques.[35] Best results are obtained for amorphous or polycrystalline films where the assumption that the quencher is miscible and randomly distributed throughout the material of interest holds.

The quencher molecule chosen should have energy levels suitable for quenching of the excited state by electron (hole) transfer in the case of donor (acceptor) type materials and should not absorb at the excitation wavelength so that excitons can selectively be generated in the host material (in this case the fullerene) only. Furthermore, minimum absorption at the emission wavelength of the host simplifies data analysis as otherwise the effects of energy transfer must also be taken into account.[35,36] For our system we chose to use tris(4-(5-phenylthiophen-2-yl)phenyl)amine (TPTPA), a star shaped triarylamine that was designed as a donor material for BHJ solar cells, and has previously been used to elucidate the exciton

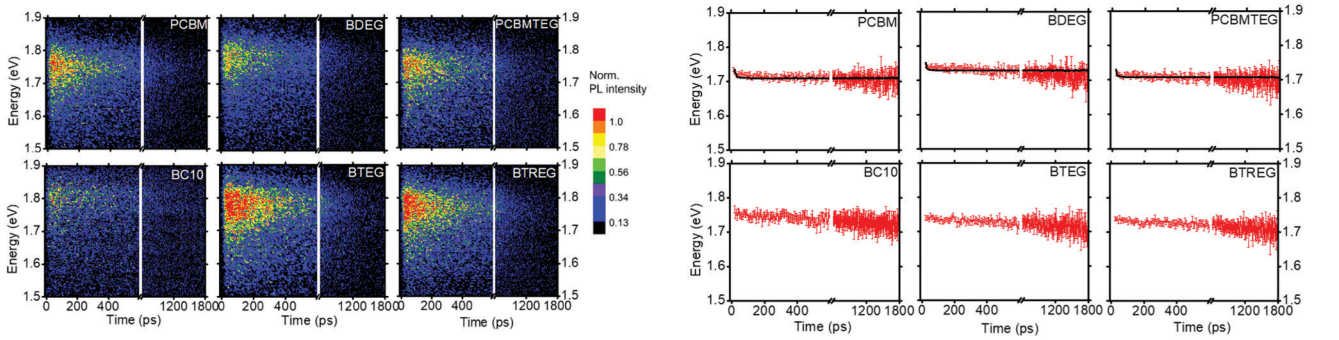

Fig. 5 Normalized PL maps for neat films of the six C_{70} derivatives (left) and the PL mean energy shift as a function of time is shown by red lines for the experimental data (right). The black lines denote the MC simulated data for [70]PCBM, PCBM-TEG and BDEG-2. The MC simulations were not carried out for the mixed films of derivatives without PL quenching (BC10-2, BTEG-2 and BTrEG-2).

diffusion length in C_{70} films.[37,38] The weight ratios of the blended films were adjusted initially using [70]PCBM until ratios were found where the quenching efficiency increased in distinct steps. Finally, blended films with weight ratios of fullerene : quencher varying from 864 : 1 to 8 : 1 (0.0012–0.13 wt%) were fabricated and the time resolved PL was measured. An excitation wavelength of 550 nm was used where TPTPA does not absorb (Fig. S12, ESI†).

The results of the PL-quenching experiments separated the six materials into two groups. For [70]PCBM, PCBM-TEG and BDEG-2, the PL decay showed the expected trend: as the quencher concentration was increased, the PL decayed faster due to quenching of the exciton by hole transfer at the fullerene: TPTPA interfaces[38] (Fig. S16, ESI†). The PL quenching efficiency (Q) was calculated using eqn (1):

$$Q = 1 - \frac{\int \mathrm{PL}_{\mathrm{blend}}\,\mathrm{d}t}{\int \mathrm{PL}_{\mathrm{neat}}\,\mathrm{d}t}$$

For the mixed blends of [70]PCBM, BDEG-2 and PCBM-TEG, the Q increases to nearly 100% with increase in quencher concentration (Fig. 6). In contrast, for BC10-2, BTEG-2 and BTREG-2 no change in the rate of PL decay was seen relative to the neat films implying a lack of quenching.

The exciton diffusion length for PCBM, PCBM-TEG and BDEG-2 could be determined by using Monte-Carlo simulations to model the PL dynamics (Section S4.1, ESI†).[39] Exciton dynamics in disordered organic systems are inherently characterized by a two step process. Initially, the exciton undergoes spectral diffusion towards lower energy sites until a quasi-equilibrium is reached at $-\sigma^2/k_BT$ below the centre of the Gaussian density of states (DOS), after which exciton diffusion proceeds *via* a thermally activated hopping mechanism.[35] The energetic disorder, $\sigma \sim 25$ meV was obtained experimentally from the PL mean energy shift (Fig. 5) and the exciton hopping time was used as the only fitting parameter for the Monte Carlo simulations and determined to be $\sim$2 ps. With these values, the experimental results were satisfactorily reproduced and an exciton diffusion length of $\sim$10 nm was calculated from the exciton displacement distribution (Fig. 6b). The diffusion coefficient (D) was initially $\sim 6.5 \times 10^{-4}$ cm^2 s^{-1} but stabilised at $D \sim 5 \times 10^{-4}$ cm^2 s^{-1} after the initial fast downhill migration through the DOS in the first 300 ps (Fig. 6c). The small magnitude of the initial drop is a result of the small energetic disorder which at $\sim$25 meV lies on the order of k_BT. These values are in agreement with previous measurements for [70]PCBM.[36,40,41]

For the other three derivatives, additional films were fabricated with fullerene:quencher ratios of 4 : 1, 2 : 1 and 1 : 1 but even at 50% quencher loading, the PL transients still showed mono-exponential decay with the same lifetime as the neat films. UV-Vis absorption spectra of the blend films confirmed that TPTPA was in fact present in the films, and there were no signs of new bands appearing in the spectra due to ground-state interactions (Section S4.2, ESI†).

We hypothesised that the lack of PL quenching could arise due to phase separation between the quencher and the fullerene derivative, negating the assumption that we are measuring homogeneous films. To gain more insight, atomic force microscopy (AFM) was used to measure the surface morphology of the films. The images of the blend films containing TPTPA show that whilst the films of [70]PCBM, PCBM-TEG and BDEG-2 (Fig. S20, ESI†) appear amorphous, the films of the other fullerene derivatives contain clear structural features in the morphology when the TPTPA concentration is increased (Fig. 7). Due to the similar photophysical properties of these three fullerenes to the others, it is reasonable to expect a similar L_D, which helps to rationalise the observed lack of quenching in the blend films since we see features in the film

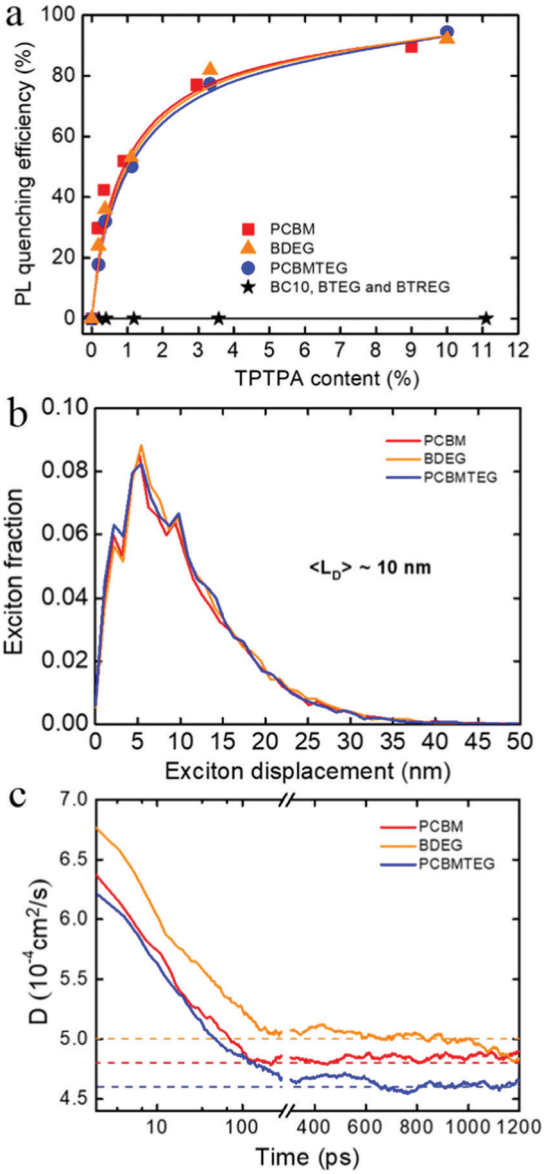

Fig. 6 (a) PL quenching efficiency *versus* TPTPA content for [70]PCBM, BDEG-2, PCBM-TEG and BC10-2/BTEG-2/BTrEG-2. The symbols represent the experimental data whereas the solid lines represent the results of the MC simulations. (b) The simulated exciton displacement distribution and (c) exciton diffusion coefficient for the [70]PCBM, BDEG-2 and PCBM-TEG films. The first 300 ps before the exciton reaches the quasi-equilibrium at $-\sigma^2/k_BT$ are shown in logarithmic scale.

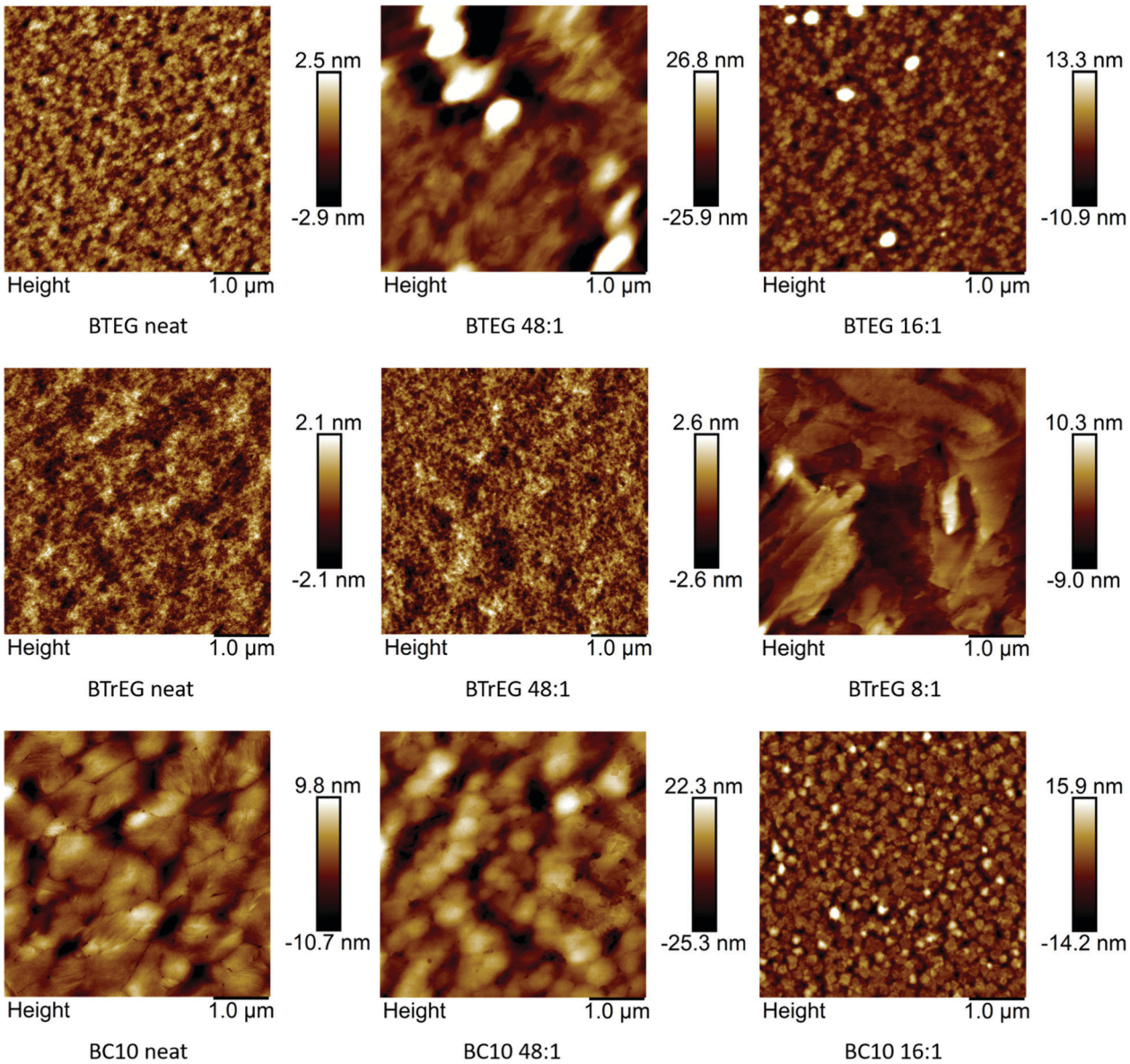

Fig. 7 AFM images of BTEG-2, BTrEG-2 and BC10-2 films containing an increasing amount (left to right) of TPTPA. The fullerene:TPTPA weight ratios are given.

morphology much larger than ~10 nm. Furthermore, in the AFM images of the neat fullerene films, the micro-crystallinity can already be observed in the films of BTEG-2 and BC10-2. This suggests that the lack of PL quenching in these mixed films is caused by the crystallinity of the fullerene derivatives which drives self assembly rather than allowing for intermixing with the TPTPA molecules. Since the fullerene domains within the film are much larger than the expected exciton diffusion length, there is a very low probability of an exciton meeting an interface with the quencher during the course of its random walk.

In an attempt to minimise phase separation, we fabricated films using a variety of spincoating conditions and solvents for BTEG-2 and BTrEG-2, with the same results (Fig. S17, ESI†). Furthermore, to test if a mismatch in the polarities of TPTPA and the fullerenes was an influencing factor, two new quencher molecules, BDT-PhTEG and 0T[42] were tested with BTEG-2 and BC10-2. BDT-PhTEG contains polar EG chains like BTEG-2 whereas 0T contains alkyl solubising chains like BC10-2. The structure of the quenchers and their UV-Vis absorption spectra are shown in Fig. S12 (ESI†). Both in the case of matched and mismatched polarities, no quenching of the fluorescence of the fullerene was detected (Fig. S19, ESI†). The presence of the quencher in the fabricated films was confirmed by measuring the absorption spectra of the films (Fig. S14 and S15, ESI†). The AFM images of the blend films with BDT-PhTEG or 0T also showed clear structural features on the film that were much larger than the predicted order of magnitude of L_D. The films are clearly micro-crystalline, and in the case of 0T, distinct aggregates appear in the blend films (Fig. S21 and S22, ESI†).

Differential scanning calorimetry (DSC) was measured on powder samples of all six derivatives, and for all the Bingel adducts, except BTrEG-2, clear endothermic/exothermic peaks could be observed that indicate reversible formation of crystalline phases. In contrast, the methano-fullerenes showed amorphous behaviour (Fig. S25, ESI†). The higher crystallinity of the Bingel adducts could arise due to the higher symmetry of their structure, as well as the fact that they are not regioisomer mixtures like [70]PCBM. In the case of BTrEG-2, although no distinct phase transitions appeared in the DSC measurement, it is likely that the length of the side chains begins to influence the exciton dynamics. In previous work, we saw as well that EG chains of length $n = 4$ (tetraethylene glycol) and longer begin to influence the charge carrier mobility of symmetrical Bingel adducts.[31]

An alternative method for measuring L_D which can be applied to neat films involves measuring the efficiency of exciton–exciton annihilation (EEA).[35] For this technique, the PL of the material is measured with increasing excitation power and once the exciton density reaches a value such that the average exciton distance is on the order of the exciton diffusion length, the PL decay begins to accelerate with further increase in power due to exciton–exciton annihilation. The diffusion coefficient can then be calculated from the measured annihilation rate constant. We measured the PL decay of BTEG-2, BTrEG-2 and BC10-2 with a range of excitation power from 10–200 μW, where 200 μW was the maximum power achievable with the experimental set-up at 550 nm. Within this range, no EEA was observed so that we could estimate an upper limit of ~30 nm on the exciton diffusion from the exciton density (Section S3.1, ESI†). We repeated these experiments with higher pulse energy at the excitation wavelength of 405 nm which allowed us to lower the no-EEA range down to 14 nm (Section S3.1, ESI†). The further increase of excitation fluence was limited by sample photodegradation which was more prominent at 405 nm than at 550 nm. Therefore, the EEA experiments place the singlet exciton diffusion length of BTEG-2, BTrEG-2 and BC10-2 within the same range as [70]PCBM.

3 Conclusions

Five new C_{70} derivatives were synthesised containing either polar (EG) or non-polar (alkyl) side-chains in order to study the link between the dielectric properties and the photophysics of the organic semiconductors. Although the ε_r^{lf} changed substantially, no correlation was found between the polarity of the side chains and the steady state absorption/emission, singlet exciton lifetime and the energetic disorder. Furthermore, the exciton diffusion length was measured and found to be the same as [70]PCBM for PCBM-TEG and BDEG-2, whilst for the others it was not possible to accurately measure the L_D with the volume-quenching method due to the microcrystalline nature of the films. Nevertheless, an upper bound on the L_D could be estimated which lies in the same order of magnitude as PCBM. These results emphasise the difficulty in correlating the properties of neat materials with the results of measurements in blend films. Since small changes in the length/polarity of side chains can have large effects on the crystallinity and morphology of different OSCs, comparison of new design principles for OSCs in terms of the PCE and performance of BHJ devices may give misleading results unless the morphology is analysed and accounted for. Regarding the effects of ε_r, future work would involve studying the effect of the side chain polarity on the triplet state photophysics, the charge carrier mobility/lifetime and on the performance of single semiconductor solar cells,[43] where it is unclear whether the micro-crystallinity observed in some of the C_{70} derivatives would be beneficial or detrimental.

4 Experimental

Materials

The detailed synthesis of BDEG-2, BTEG-2, BTrEG-2, BC10-2 and PCBM-TEG is described in the ESI.† C_{70} and [70]PCBM were purchased from Solenne B.V. (Groningen). TPTPA was purchased from LumTec Corp. and used as received. 0T[42] and BDT-PhTEG[44] were synthesised following the procedure from the literature.

Impedance spectroscopy

The following procedure was carried out in the clean room. Commercially available glass substrates patterned with indium-tin-oxide (ITO) were used for all capacitors. The substrates were scrubbed with soapy water, rinsed with de-ionised water, sonicated in acetone (10 min) and isopropanol (15 min), spin dried, further dried in an oven at 140 °C for 10 minutes and subjected to 20 minutes of UV-ozone treatment before use. PEDOT:PSS water dispersion (VP AI4083, H. C. Stark) was filtered through PTFE filters (0.45 μm), spin-cast in ambient conditions and annealed in the oven at 140 °C for 10 minutes. All fullerene derivatives were spin-cast from anhydrous solutions under an N_2 atmosphere in the glovebox, the spincoating program was varied to achieve different thicknesses. Aluminium top electrodes were deposited by thermal evaporation at a pressure less than 10^{-6} mbar. The impedance was measured in a two electrode configuration using a Solartron 1260 impedance analyser with an applied AC voltage signal of 10–20 mV. The series resistance of the cables was fitted in the equivalent circuit used for data analysis and varied from 20–100 Ω. The thickness was measured using a DEKTAK profilometer, after scratching the films with a glass pipette. The PEDOT:PSS thickness was obtained from an extra ITO/PEDOT:PSS sample that was prepared on the same day as the capacitor devices, and substracted to obtain the thickness of the fullerene layer.

Film preparation

Glass substrates (17 mm × 13 mm) were cleaned by scrubbing with soapy water (Extran MA 02, Sigma Aldrich), rinsing 3× with demi water, sonicating in acetone (10 min) and in isopropanol (15 min). After this, the substrates were dried individually with a

nitrogen gun, placed in the oven for 10 minutes at 120 °C and treated with O_2 plasma for three minutes. The films were spin-coated in the clean room but under ambient conditions using a two step program: (1) 500 rpm, 1000 rpm s^{-1}, 40 s then (2) 1000 rpm, 1000 rpm s^{-1}, 10 s. For the EEA measurements with excitation at 405 nm, the samples were prepared following the same procedure but on quartz substrates instead (10 mm × 10 mm).

The solutions for the neat films varied in concentration between 6–12 mg mL^{-1}. The blend solutions were made by mixing a 16 mg mL^{-1} fullerene solution with a solution of the quencher in a 3 : 1 ratio in order to keep the concentration of the fullerene fixed at 12 mg mL^{-1}. The concentration of the quencher solution was varied to achieve the desired ratio, *e.g.* for an 8 : 1 ratio a 6 mg mL^{-1} solution of the quencher was used. The solvents used were spectroscopy grade.

Ellipsometry

Ellipsometry measurements were carried out on a J. A. Woollam VB-400 spectroscopic ellipsometer with a HS-190 control unit/monochromator. Each sample was measured in two different spots at three incident angles in the spectral range 400–1700 nm. The back of the glass substrates was covered in black tape so as to prevent reflection from the glass–air interface at the back of the sample, allowing us to assume no back reflection from the bottom interface for our optical model. The optical models were constructed and fitted using J. A. Woollam's WVASE software with the Cauchy or GenOsc material model.

Spectroscopic measurements

UV-Vis absorption spectra in solution and of the blend films were measured on a Jenway 6715 UV/Vis spectrophotometer. The neat film absorption spectra were measured in reflectance mode on a JASCO V-570 UV-Vis-NIR spectrometer fitted with an integrating sphere.

Time resolved photoluminescence data were acquired using a streak camera (C5680 from Hamamatsu) equipped with a spectrograph. The excitation wavelength was obtained by focusing the output from the mode-locked Ti:sapphire laser (Mira 900) into the Newport SGC-800 hollow fiber and selecting the portion of the white light with a band pass filter of 550 nm central wavelength and FWHM of 10 nm. The excitation power was 50 μW. A long pass filter (OG 610) was placed before the spectrograph to filter residual excitation light. For the EEA experiments, the second harmonic of the fundamental radiation (wavelength 405 nm) was also used. The experimental time resolution was ∼10 ps.

Film morphology

AFM images were measured using a Bruker Multimode in Scanasyst mode with Scanasyst-Air tips.

Author contributions

S. R. and J. C. H. designed the materials and conceptualised goals for the project with suggestions from M. S. P. S. R. and F. S. v. K. synthesised and fully characterised the C_{70} derivatives, fabricated devices and measured their dielectric properties. S. R. obtained and fitted the ellipsometry data, prepared the blend films, measured the UV-Vis absorption spectra and AFM images. B. A. L. R. carried out the PL measurements and MC simulations while A. V. K. performed the EEA experiments at 405 nm; both under the guidance of M. S. P. S. B. synthesised BDT-PhTEG under the supervision of R. C. C. S. R. wrote the manuscript supervised by R. C. C. with contributions from B. A. L. R. and input from the other authors.

Conflicts of interest

There are no conflicts to declare.

Acknowledgements

This work is part of the research program of the Foundation for Fundamental Research on Matter (FOM), which is part of The Netherlands Organization for Scientific Research (NWO). This publication is part of the work of the FOM Focus Group 'Next Generation Organic Photovoltaics', participating in the Dutch Institute for Fundamental Energy Research (DIFFER). B. A. L. R. and M. S. P. acknowledge funding from the European Union's Horizon 2020 research and innovation programme under the Marie Skłodowska-Curie grant agreement 722651 (SEPOMO). The authors thank A. F. Kamp. T. Zaharia, F. de Haan and B. Visser for their technical assistance with the equipment in the clean room and in the measurement labs. B. A. L. R. and M. S. P. also thank F. de Haan for writing the Monte Carlo simulation code. The authors thank the Enikolopov Institute of Synthetic Polymeric Materials of the Russian Academy of Sciences, Moscow, Russia for providing the quencher molecule 0T.

References

1 G. Yu, J. Gao, J. C. Hummelen, F. Wudl and A. J. Heeger, *Science*, 1995, **270**, 1789–1791.
2 P. R. Berger and M. Kim, *J. Renewable Sustainable Energy*, 2018, **10**, 013508.
3 R. Ganesamoorthy, G. Sathiyan and P. Sakthivel, *Solar Energy Mater. Sol. Cells*, 2017, **161**, 102–148.
4 S. Cook, H. Ohkita, Y. Kim, J. J. Benson-Smith, D. D. Bradley and J. R. Durrant, *Chem. Phys. Lett.*, 2007, **445**, 276–280.
5 H. Wang, Y. He, Y. Li and H. Su, *J. Phys. Chem. A*, 2011, **116**, 255–262.
6 C. Keiderling, S. Dimitrov and J. R. Durrant, *J. Phys. Chem. C*, 2017, **121**, 14470–14475.
7 S. Karuthedath, J. Gorenflot, Y. Firdaus, W.-Y. Sit, F. Eisner, A. Seitkhan, M. K. Ravva, T. D. Anthopoulos and F. Laquai, *Adv. Energy Mater.*, 2018, **9**, 1802476.
8 A. Serbenta, O. V. Kozlov, G. Portale, P. H.-M. van Loosdrecht and M. S. Pshenichnikov, *Sci. Rep.*, 2016, **6**, 36236.
9 T. Albes, L. Xu, J. Wang, J. W.-P. Hsu and A. Gagliardi, *J. Phys. Chem. C*, 2018, **122**, 15140–15148.

10 W. Kaiser, L. N.-S. Murthy, C.-L. Chung, K.-T. Wong, J. W. Hsu and A. Gagliardi, *Adv. Energy Sustainability Res.*, 2021, **2**, 2000042.
11 N. Gasparini, A. Salleo, I. McCulloch and D. Baran, *Nat. Rev. Mater.*, 2019, **4**, 229–242.
12 J.-W. van der Horst, P. A. Bobbert, M. A.-J. Michels and H. Bässler, *J. Chem. Phys.*, 2001, **114**, 6950–6957.
13 L. J.-A. Koster, S. E. Shaheen and J. C. Hummelen, *Adv. Energy Mater.*, 2012, **2**, 1246–1253.
14 J. Brebels, J. V. Manca, L. Lutsen, D. Vanderzande and W. Maes, *J. Mater. Chem. A*, 2017, **5**, 24037–24050.
15 V. Ivasyshyn, G. Ye, S. Rousseva, J. C. Hummelen and R. C. Chiechi, *Increasing the Dielectric Constant of Organic Materials for Photovoltaics*, 2018, DOI: **10.1002/9781119407690.ch11**.
16 Z. Fu, X. Zhang, H. Zhang, Y. Li, H. Zhou and Y. Zhang, *Chin. J. Chem.*, 2020, **39**, 381–390.
17 B. Xu, X. Yi, T.-Y. Huang, Z. Zheng, J. Zhang, A. Salehi, V. Coropceanu, C. H.-Y. Ho, S. R. Marder, M. F. Toney, J.-L. Brédas, F. So and J. R. Reynolds, *Adv. Funct. Mater.*, 2018, **28**, 1803418.
18 M. P. Hughes, K. D. Rosenthal, R. R. Dasari, B. R. Luginbuhl, B. Yurash, S. R. Marder and T.-Q. Nguyen, *Adv. Funct. Mater.*, 2019, **29**, 1901269.
19 A. Armin, D. M. Stoltzfus, J. E. Donaghey, A. J. Clulow, R. C.-R. Nagiri, P. L. Burn, I. R. Gentle and P. Meredith, *J. Mater. Chem. C*, 2017, **5**, 3736–3747.
20 S. Sami, P. A. Haase, R. Alessandri, R. Broer and R. W. Havenith, *J. Phys. Chem. A*, 2018, **122**, 3919–3926.
21 R. Kerremans, C. Kaiser, W. Li, N. Zarrabi, P. Meredith and A. Armin, *Adv. Opt. Mater.*, 2020, **8**, 2000319.
22 L. Duan, C. Xu, H. Yi, M. B. Upama, M. A. Mahmud, D. Wang, F. Haque and A. Uddin, *IEEE J. Photovoltaics*, 2019, **9**, 1031–1039.
23 P. Li, J. Fang, Y. Wang, S. Manzhos, L. Cai, Z. Song, Y. Li, T. Song, X. Wang, X. Guo, M. Zhang, D. Ma and B. Sun, *Angew. Chem., Int. Ed.*, 2021, **60**, 15054–15062.
24 T. Umeyama, T. Miyata, A. C. Jakowetz, S. Shibata, K. Kurotobi, T. Higashino, T. Koganezawa, M. Tsujimoto, S. Gélinas, W. Matsuda, S. Seki, R. H. Friend and H. Imahori, *Chem. Sci.*, 2017, **8**, 181–188.
25 T. Umeyama and H. Imahori, *Acc. Chem. Res.*, 2019, **52**, 2046–2055.
26 C. Bingel, *Chem. Ber.*, 1993, **126**, 1957–1959.
27 A. Herrmann, M. Rüttimann, C. Thilgen and F. Diederich, *Helv. Chim. Acta*, 1995, **78**, 1673–1704.
28 S. Torabi, J. Liu, P. Gordiichuk, A. Herrmann, L. Qiu, F. Jahani, J. C. Hummelen and L. J.-A. Koster, *ACS Appl. Mater. Interfaces*, 2016, **8**, 22623–22628.
29 S. Torabi, M. Cherry, E. A. Duijnstee, V. M.-L. Corre, L. Qiu, J. C. Hummelen, G. Palasantzas and L. J.-A. Koster, *ACS Appl. Mater. Interfaces*, 2017, **9**, 27290–27297.
30 M. P. Hughes, K. D. Rosenthal, N. A. Ran, M. Seifrid, G. C. Bazan and T.-Q. Nguyen, *Adv. Funct. Mater.*, 2018, **28**, 1801542.
31 S. Rousseva, H. den Besten, F. S. van Kooij, E. L. Doting, N. Y. Doumon, E. Douvogianni, L. J.-A. Koster and J. C. Hummelen, *J. Phys. Chem. C*, 2020, **124**, 8633–8638.
32 F. B. Aboura, D. Duché, J. Simon and L. Escoubas, *Chem. Phys.*, 2015, **450-451**, 102–108.
33 J. W. Arbogast and C. S. Foote, *J. Am. Chem. Soc.*, 1991, **113**, 8886–8889.
34 P. S. Marqués, J. M.-A. Castán, B. A.-L. Raul, G. Londi, I. Ramirez, M. S. Pshenichnikov, D. Beljonne, K. Walzer, M. Blais, M. Allain, C. Cabanetos and P. Blanchard, *Chem. – Eur. J.*, 2020, **26**, 16422–16433.
35 O. V. Mikhnenko, P. W.-M. Blom and T.-Q. Nguyen, *Energy Environ. Sci.*, 2015, **8**, 1867–1888.
36 G. J. Hedley, A. J. Ward, A. Alekseev, C. T. Howells, E. R. Martins, L. A. Serrano, G. Cooke, A. Ruseckas and I. D.-W. Samuel, *Nat. Commun.*, 2013, **4**, 2867.
37 H. Kageyama, H. Ohishi, M. Tanaka, Y. Ohmori and Y. Shirota, *Appl. Phys. Lett.*, 2009, **94**, 063304.
38 O. V. Kozlov, F. de Haan, R. A. Kerner, B. P. Rand, D. Cheyns and M. S. Pshenichnikov, *Phys. Rev. Lett.*, 2016, **116**, 057402.
39 B. A.-L. Raul, Y. N. Luponosov, W. Yang, N. M. Surin, O. Douhéret, J. Min, T. L.-C. Jansen, S. A. Ponomarenko and M. S. Pshenichnikov, *Sci. Rep.*, 2020, **10**, 21198.
40 N. Zarrabi, A. Yazmaciyan, P. Meredith, I. Kassal and A. Armin, *J. Phys. Chem. Lett.*, 2018, **9**, 6144–6148.
41 Y. Firdaus, V. M.-L. Corre, S. Karuthedath, W. Liu, A. Markina, W. Huang, S. Chattopadhyay, M. M. Nahid, M. I. Nugraha, Y. Lin, A. Seitkhan, A. Basu, W. Zhang, I. McCulloch, H. Ade, J. Labram, F. Laquai, D. Andrienko, L. J.-A. Koster and T. D. Anthopoulos, *Nat. Commun.*, 2020, **11**, 2867.
42 Y. N. Luponosov, A. N. Solodukhin, A. L. Mannanov, P. S. Savchenko, B. A. Raul, S. M. Peregudova, N. M. Surin, A. V. Bakirov, M. A. Shcherbina, S. N. Chvalun, M. S. Pshenichnikov, D. Y. Paraschuk and S. A. Ponomarenko, *Materials Today Energy*, 2021, **22**, 100863.
43 J. Roncali and I. Grosu, *Adv. Sci.*, 2018, **6**, 1801026.
44 L. Ye, S. Zhang, L. Huo, M. Zhang and J. Hou, *Acc. Chem. Res.*, 2014, **47**, 1595–1603.

